

# Reactive Zr<sup>IV</sup> and Hf<sup>IV</sup> Butterfly Peroxides on Polyoxometalate Surfaces: Bridging the Gap between Homogeneous and Heterogeneous Catalysis

Mauro Carraro,<sup>\*,[a]</sup> Nadeen Nsouli,<sup>[b]</sup> Holger Oelrich,<sup>[c]</sup> Andrea Sartorel,<sup>[a]</sup>  
Antonio Sorarù,<sup>[a]</sup> Sib Sankar Mal,<sup>[b]</sup> Gianfranco Scorrano,<sup>[a]</sup> Lorenz Walder,<sup>\*,[c]</sup>  
Ulrich Kortz,<sup>\*,[b]</sup> and Marcella Bonchio<sup>\*,[a]</sup>

**Abstract:** At variance with previously known coordination compounds, the polyoxometalate (POM)-embedded Zr<sup>IV</sup> and Hf<sup>IV</sup> peroxides with formula: [M<sub>2</sub>(O<sub>2</sub>)<sub>2</sub>(α-XW<sub>11</sub>O<sub>39</sub>)<sub>2</sub>]<sup>12-</sup> (M = Zr<sup>IV</sup>, X = Si (1), Ge (2); M = Hf<sup>IV</sup>, X = Si (3)) and [M<sub>6</sub>(O<sub>2</sub>)<sub>6</sub>(OH)<sub>6</sub>(γ-SiW<sub>10</sub>O<sub>36</sub>)<sub>3</sub>]<sup>18-</sup> (M = Zr<sup>IV</sup> (4) or Hf<sup>IV</sup> (5)) are capable of oxygen transfer to suitable acceptors including sulfides and sulfoxides in water. Combined <sup>1</sup>H NMR and electrochemical studies allow monitoring of the reaction under both stoichiometric and catalytic conditions. The reactivity of peroxo-POMs 1–5 is compared on the basis of substrate conversion and

kinetic. The results show that the reactivity of POMs 1–3 outperforms that of the trimeric derivatives 4 and 5 by two orders of magnitude. Reversible peroxidation of 1–3 occurs by H<sub>2</sub>O<sub>2</sub> addition to the spent catalysts, restoring oxidation rates and performance of the pristine system. The stability of 1–3 under catalytic regime has been confirmed by FT-IR, UV/Vis, and resonance Raman spectroscopy. The reaction scope has

been extended to alcohols, leading to the corresponding carbonyl compounds with yields up to 99% under microwave (MW) irradiation. DFT calculations revealed that polyanions 1–3 have high-energy peroxo HOMOs, and a remarkable electron density localized on the peroxo sites as indicated by the calculated map of the electrostatic potential (MEP). This evidence suggests that the overall description of the oxygen-transfer mechanism should include possible protonation equilibria in water, favored for peroxo-POMs 1–3.

**Keywords:** hafnium • homogeneous catalysis • oxidation • peroxides • polyoxometalates • zirconium

## Introduction

Though solid metal oxides, including zirconia-based catalysts, are considered interesting in oxidation catalysis,<sup>[1]</sup> limited knowledge is available on the structural and electronic properties of surface-anchored peroxo sites that have been postulated as competent oxidants.<sup>[2,3]</sup> In a few cases, stable monoperoxo complexes of Zr<sup>IV</sup> have been isolated by reac-

tion with H<sub>2</sub>O<sub>2</sub>, in the presence of nitrogen–oxygen/sulphur donor ligands.<sup>[4,5]</sup> Of major importance is the access to Zr<sup>IV</sup> peroxides by ligand-mediated O<sub>2</sub> activation, as demonstrated by the work of Abu-Omar et al., in which an η<sup>2</sup>-bisperoxo complex containing bidentate diimines was obtained.<sup>[6]</sup> However, the so-far characterized Zr<sup>IV</sup>-peroxo complexes, featuring multidentate organic ligands, are catalytically inert towards the oxidation of organic substrates, such as phosphines, alkenes, and alcohols.<sup>[4,5]</sup> Hf<sup>IV</sup> analogues are even less documented. An interesting discovery is the structural characterization of peroxo-bridged Hf<sup>IV</sup> tetraarylporphyrinato dimers, displaying two O<sub>2</sub><sup>2-</sup> ligands with a rather unique, side-on bis-μ-η<sup>2</sup>:η<sup>2</sup> arrangement.<sup>[7]</sup>

The introduction of Zr<sup>IV</sup> and Hf<sup>IV</sup> ions within the framework of polyoxometalates (POMs) of W<sup>VI</sup> and Mo<sup>VI</sup> has also been reported, in which M-(μ-O)-M (M = Zr<sup>IV</sup>, Hf<sup>IV</sup>) junctions promote the formation of oligomeric structures.<sup>[8]</sup> Due to the large size of Zr<sup>IV</sup> and Hf<sup>IV</sup> ions, coordination numbers up to seven can be accessed, including one or more terminal water molecules. This structural feature is expected to boost catalysis by providing accessible and adjacent sites for ligand exchange, becoming available for simultaneous substrate and peroxide activation at the metal center.<sup>[9]</sup> In this chemistry, the POM framework can offer some key improvements being a totally inorganic, highly robust, and electron-withdrawing environment, with structural and coordination properties modeling a discrete fragment of solid

[a] Dr. M. Carraro, Dr. A. Sartorel, A. Sorarù, Prof. G. Scorrano, Dr. M. Bonchio  
Department of Chemical Sciences  
ITM-CNR and University of Padova  
Via Marzolo 1, 35131 Padova (Italy)  
E-mail: mauro.carraro@unipd.it  
marcella.bonchio@unipd.it

[b] Dr. N. Nsouli, Dr. S. S. Mal, Prof. U. Kortz  
School of Engineering and Science  
Jacobs University  
P.O. Box 750 561, 28725, Bremen (Germany)  
E-mail: u.kortz@jacobs-university.de

[c] Dr. H. Oelrich, Prof. L. Walder  
Institute of Chemistry, University of Osnabrück  
Barbarastrasse 7, 49069 Osnabrück (Germany)  
E-mail: LoWalder@uos.de

Supporting Information for this article (kinetic data obtained from <sup>1</sup>H NMR and electrochemical data; Cartesian coordinates corresponding to the optimized geometries of 1–5) is available on the WWW under <http://dx.doi.org/10.1002/chem.201003103>.

metal oxides.<sup>[10]</sup> In this respect, Zr and Ti-based POMs have been suggested as molecular models for the well-known heterogeneous titanium silicalite catalyst, TS-1, with major industrial appeal in the field of H<sub>2</sub>O<sub>2</sub> activation and selective oxidation.<sup>[8i,11]</sup> On the other hand, transition-metal-substituted POMs can mimic the active site geometry of natural oxygenases.<sup>[9,12–14]</sup> Indeed, nature's strategy to face some formidable catalytic challenges is the stabilization of adjacent transition-metal centers through multiple- $\mu$ -hydroxo/oxo bridging units, that is, the basic structural motif of the POM molecular connectivity.

We have recently reported the structural characterization and preliminary catalytic studies of novel heteropolytungstates incorporating Zr<sup>IV</sup> and Hf<sup>IV</sup> peroxides. These are unique examples of bimetallic peroxides, having so-called butterfly-type cores with a mono- or bis- $\mu$ - $\eta^2$ : $\eta^2$  arrangement of the peroxo ligand for each Zr/Hf center embedded within the POM scaffold (Figure 1).<sup>[15,16]</sup>

Such a structural feature is shared by three isostructural dimers,  $[[M(O_2)(\alpha-XW_{11}O_{39})_2]^{12-}]$  (M=Zr, X=Si (1), Ge (2); M=Hf, X=Si (3)),<sup>[15]</sup> and by the trimeric derivatives

$[M_6(O_2)_6(OH)_6(\gamma-SiW_{10}O_{36})_3]^{18-}$  (M=Zr (4) or Hf (5)) displaying a cyclic 6-peroxo-6-metal core stabilized by three decatungstosilicate units (Figure 1).<sup>[16]</sup>

We present herein a combined kinetic, electrochemical, and computational study to investigate the potential of Zr/Hf butterfly peroxides for oxygen transfer in water, under stoichiometric and catalytic regimes. Our results highlight the role of the POM ligand powering the reactivity of the Zr/Hf peroxides, in contrast with the generally found inertness of related classical coordination compounds. The results presented herein point to structure–reactivity correlations in the realm of functional metal oxides. These are instrumental for the rational design and synthesis of innovative ligands/catalysts taken from the POM pool and their further upgrade to molecular materials.<sup>[17,18]</sup>

## Results and Discussion

The peroxo functions of complexes 1–5 are readily reduced by iodide in water, and they can be thus quantitatively titrated by a standard thiosulfate solution. Reductive expulsion of the peroxo functions is also observed by cyclic voltammetry (two e<sup>-</sup> per peroxo function). This fact allows to determine the ratio of peroxo POM to peroxo-free POM in a simple double scan on the reductive wave appearing at  $\approx -0.8$  V (vs. Ag/AgCl, see Figures S1–S5 in the Supporting Information).<sup>[15,19]</sup> The reactivity of POMs 1–5 has been assessed for oxygen transfer to L-methionine (S) in aqueous solution. This benchmark transformation occurs through the mono- and bis-oxygenation of the sulfur atom, yielding the sulfoxide (SO) and sulfone (SO<sub>2</sub>) products, respectively (Figure 1). Such a consecutive two-step process has been monitored with complementary <sup>1</sup>H NMR and fast electrochemical scanning techniques, by following the substrate/product time-evolution or the fading of the peroxo-POM concentration, respectively, upon oxygen transfer. In particular, <sup>1</sup>H NMR analysis provides direct evidence of the oxidation yield and product distribution as diagnostic signals are found at 2.1, 2.6, and 3.2 ppm attributed to the S, SO and SO<sub>2</sub> terminal methyl groups, respectively (Figure S6 in the Supporting Information). On the other hand, voltammetric analysis, also implemented with rotating disk setup at a fixed potential ( $E = -0.85$  V), adds a convergent scenario indicating the progressive quenching of the peroxo functionality upon stepwise addition of L-methionine (Figure 2 and Figures S7–S12 in the Supporting Information).<sup>[20]</sup>

This combined screening strategy allows us to match the diverse kinetic domains of the oxidation experiments, spanning from a few seconds to hundreds of minutes, depending on the reactivity behavior of the complexes under examination. In particular, fast kinetics that could not be successfully accomplished by means of conventional <sup>1</sup>H NMR methods have been addressed by rotating disk voltammetry (vide infra and Table 1). The reactivity of peroxo-POMs 1–5 is compared in Table 1 on the basis of substrate conversion and kinetic data. In such a two-step process, the selectivity

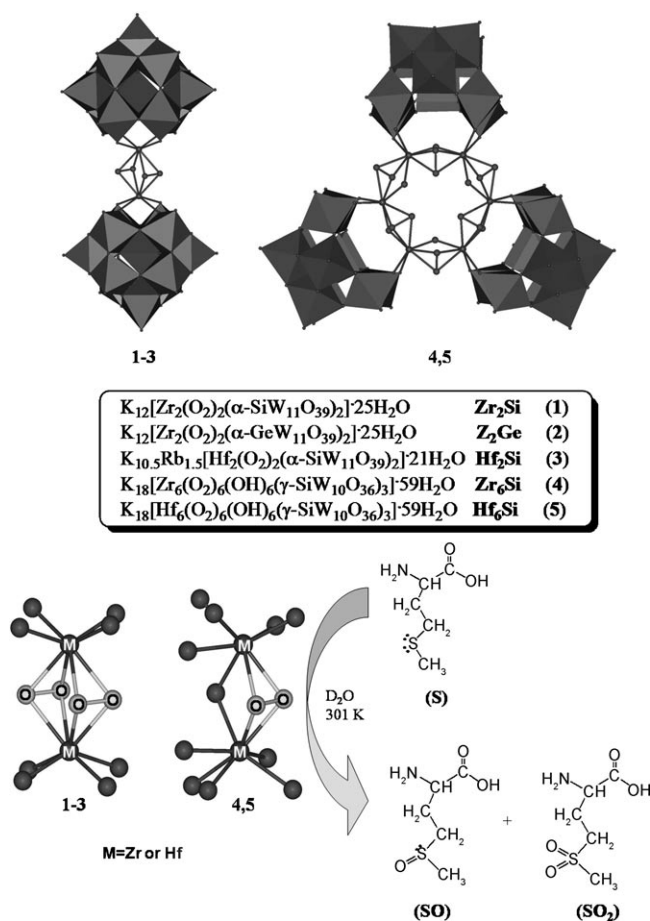


Figure 1. Combined polyhedral/ball-and-stick representation of  $[[M(O_2)(\alpha-XW_{11}O_{39})_2]^{12-}]$  (M=Zr, X=Si (1), Ge (2); M=Hf, X=Si (3)), and of  $[M_6(O_2)_6(OH)_6(\gamma-SiW_{10}O_{36})_3]^{18-}$  (M=Zr (4) or Hf (5)). The reaction scheme represents the oxygen transfer to L-methionine (S) to give DL-methionine sulfoxide (SO) and methionine sulfone (SO<sub>2</sub>).

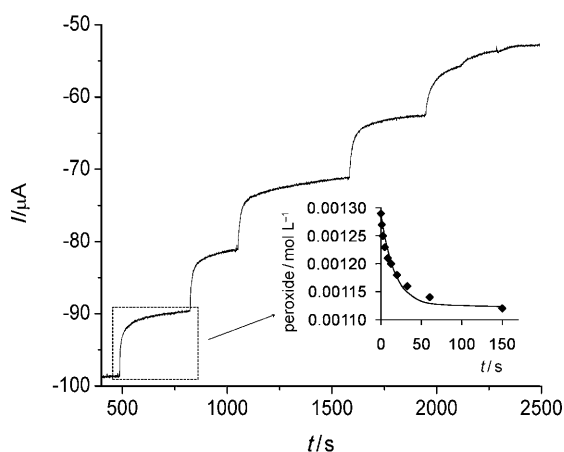


Figure 2. Rotating disk voltammetry of **1** ( $n=3.86 \mu\text{mol}$ ,  $6.43 \times 10^{-4} \text{M}$ ) during substoichiometric additions of L-methionine ( $1 \mu\text{mol}$  portions) in  $0.5 \text{M}$  HAc/KAc buffer (pH 4.7) at a glassy carbon electrode ( $A=0.07 \text{cm}^2$ ) and a fixed potential ( $E=-0.85 \text{V}$ ). Inset: kinetic trace of peroxide consumption derived from the first step of the current/time plot.

Table 1. Oxidation of L-methionine (**S**) and/or DL-methionine oxide (**SO**) by peroxo-POMs **1–5** in aqueous solution.<sup>[a]</sup>

	Sub	POM <sup>[b]</sup>	Time [min]	Conv. [%] <sup>[c]</sup>	Initial rate, $R_0$ [mol L <sup>-1</sup> s <sup>-1</sup> ] <sup>[e]</sup>
1	<b>S</b>	<b>1</b> (Zr <sub>2</sub> Si)	<1	>99 <sup>[d]</sup>	$2.7 \times 10^{-3[f]}$
2	<b>S</b>	<b>2</b> (Zr <sub>2</sub> Ge)	<1	>99 <sup>[d]</sup>	$1.8 \times 10^{-3[f]}$
3	<b>S</b>	<b>3</b> (Hf <sub>2</sub> Si)	<1	>99 <sup>[d]</sup>	$3.1 \times 10^{-3[f]}$
4	<b>S</b>	<b>4</b> (Zr <sub>6</sub> Si)	240	97 <sup>[d]</sup>	$1.0 \times 10^{-5}$
5	<b>S</b>	<b>5</b> (Hf <sub>6</sub> Si)	50	99 <sup>[d]</sup>	$3.9 \times 10^{-5}$
6	<b>SO</b>	<b>1</b> (Zr <sub>2</sub> Si)	90	94 <sup>[g]</sup>	$1.1 \times 10^{-5[h]}$
7 <sup>[h]</sup>	<b>SO</b>	<b>1</b> (Zr <sub>2</sub> Si)	90	94 <sup>[g]</sup>	$1.0 \times 10^{-5}$
8	<b>SO</b>	<b>2</b> (Zr <sub>2</sub> Ge)	120	83 <sup>[g]</sup>	$6.8 \times 10^{-6[i]}$
9 <sup>[h]</sup>	<b>SO</b>	<b>2</b> (Zr <sub>2</sub> Ge)	120	87 <sup>[g]</sup>	$6.6 \times 10^{-6}$
10	<b>SO</b>	<b>3</b> (Hf <sub>2</sub> Si)	60	88 <sup>[g]</sup>	$1.4 \times 10^{-5[j]}$
11 <sup>[h]</sup>	<b>SO</b>	<b>3</b> (Hf <sub>2</sub> Si)	60	96 <sup>[g]</sup>	$1.3 \times 10^{-5}$

[a] In all reactions stoichiometric substrate (Sub) and peroxide content ( $O_{\text{acc}}$ ) have been established vis-à-vis the dimeric or trimeric structure of POMs **1–5** ( $[\text{Sub}] = [O_{\text{acc}}] = 7.27 \text{mM}$ , in  $D_2O$  (500  $\mu\text{L}$ ), at  $28^\circ\text{C}$ ). [b] See Figure 1 for POM abbreviations. [c] % Substrate conversion. [d] Selective **SO** formation as determined by  $^1\text{H}$  NMR spectroscopy. [e] Initial oxidation rate, determined for <15% conversion by  $^1\text{H}$  NMR spectroscopy. [f] Initial oxidation rate, determined by rotating disk voltammetry (see Experimental Section). [g] Selective **SO**<sub>2</sub> formation as determined by  $^1\text{H}$  NMR spectroscopy. [h] Recharge experiments, with further addition of **SO** and  $\text{H}_2\text{O}_2$  to restore their initial amounts (3.63  $\mu\text{mol}$ ). [i] Fitting of CV data provide  $R_0 = 1.8 \times 10^{-5}$ ,  $1.0 \times 10^{-5}$ ,  $1.2 \times 10^{-5} \text{mol L}^{-1} \text{s}^{-1}$  for POMs **1–3**, respectively, (see Experimental Section).

of the oxidation depends on the relative reactivity of the Zr/Hf peroxides towards the sulfide and the sulfoxide functional groups.<sup>[21,22]</sup> Under stoichiometric conditions, complexes **1–5** all display a remarkable activity towards **S** oxidation, yielding quantitative oxygen transfer to the electron-rich sulfur atom (entries 1–5 in Table 1), to give **SO** as the only product (see Experimental Section for the detailed procedure). In particular, sulfoxidation by polyanions **1–3** is complete within seconds. In this time-frame, rotating disk voltammetry was used to gain further evidence by kinetic fitting of the reaction transients, as depicted in Figure 2 for

complex **1** (see Experimental Section). Concerning the oxygen-transfer rate, POMs **1–3** turn out to outmatch the trimeric derivatives **4** and **5** by two orders of magnitude (entries 1–3 vs. 4 and 5 in Table 1). While the nature of both the Hf or Zr center and POM ligand plays a minor role, a major impact on reactivity stems from the coordination mode and structural environment of the Zr/Hf peroxides. In this regard, the bis- $\mu$ - $\eta^2$ : $\eta^2$  peroxides **1–3**, in which each Zr/Hf center is connected by four M-O-W bonds to the POM scaffold, are powerful electrophiles, and hence more reactive sulfoxidation reagents than the related trimers. These trimers have a looser connectivity to the Group IV heterometals with just two M-O-W units per each Hf/Zr center.

The superior reactivity of the bis- $\mu$ - $\eta^2$ : $\eta^2$ -peroxides **1–3** is also apparent in the second oxidation, converting **SO** to **SO**<sub>2</sub>. Indeed, overoxidation to **SO**<sub>2</sub> can be achieved with POMs **1–3** (entries 6, 8, 10 in Table 1), while it is negligible with complexes **4** and **5**. Polyanions **1–3** behave as electrophilic oxidants, displaying an enhanced reactivity towards the electron-rich thioether with respect to the sulfoxide moiety.<sup>[21]</sup> In this respect, a reactivity ratio of  $\text{S}/\text{SO} > 100$  can be calculated on the basis of the oxidation rates determined for all complexes (entries 1–3 and 6, 8, 10 in Table 1). This is also consistent with the sharp selectivity favoring the first step of the oxidation, that is, the sulfoxide production (entries 1–3 in Table 1).<sup>[21b]</sup> Oxygen transfer to **SO** by POMs **1–3** has been further investigated monitoring the time profile of simultaneous **SO** conversion and peroxide consumption by  $^1\text{H}$  NMR and voltammetric analysis, respectively (Figure S13–S26 in the Supporting Information). Upon comparison of the oxidation rates observed for **1–3**, the tungstosilicate ligand performs slightly better than the germanate analogue, while the Hf and Zr species behave similarly (entries 6, 8, 10 in Table 1). To get further mechanistic insights, a set of reactions with variable concentration of **3** has been carried out and monitored by  $^1\text{H}$  NMR spectroscopy (Figure 3).

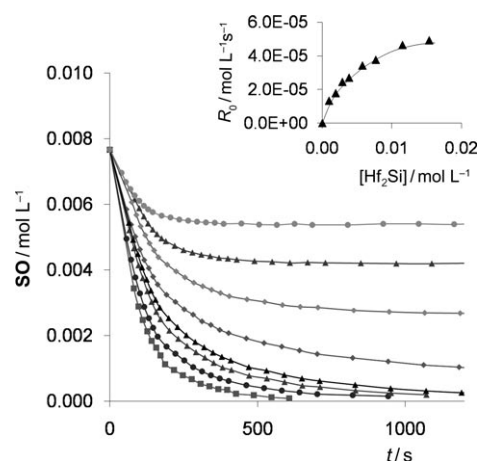


Figure 3. Kinetic traces obtained during oxidation of **SO** (7.27 mM) with **3**, in the concentration range (0.958–15.3 mM; top to bottom). Inset: dependence of the initial oxidation rates ( $R_0$ ) on the concentration of **3**.

Increasing the concentration of the POM leads to rate saturation (inset in Figure 3), which is generally indicative of association pre-equilibria. Indeed, as the reaction pH is close to the isoelectric point of methionine ( $pI=5.74$ ), an electrostatic interaction between the anionic POM and the protonated amino group of the substrate can be envisaged. Complementary charge interactions are known to affect the reactivity and selectivity of POM reagents both in aqueous solution and in organic solvents.<sup>[23]</sup>

After oxygen transfer, the stability of the spent peroxo-POMs has been confirmed by FT-IR, UV/Vis, and resonance Raman analysis.<sup>[24]</sup> Superimposable spectra are shown in Figure 4 for the representative case of POM **3** (see also

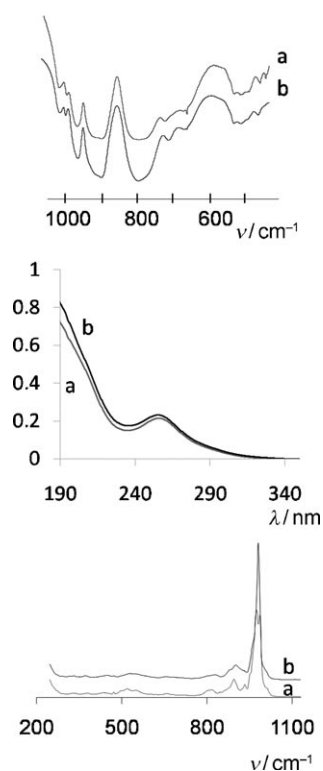


Figure 4. FT-IR (top), UV/Vis (middle), and resonance Raman spectra (bottom) of **3** a) before and b) after the reaction with L-methionine. Reactions performed under the experimental conditions described for entry 10 in Table 1.

Figures S27–S29 and S32–S34 in the Supporting Information). The structural integrity of POM **1–3** scaffold is generally confirmed by multiple techniques. The resonance Raman spectrum shows very weak signals at 550–650  $\text{cm}^{-1}$ , the expected region for  $M(\text{O}_2)$  absorption, while the sharpening of the 980  $\text{cm}^{-1}$  feature, in the region of  $\text{W}=\text{O}$  bands, is likely induced by the reversible rearrangement of the POM scaffold upon peroxide reduction.<sup>[8h,25]</sup>

The maintenance of the POM framework is pivotal for the upgrade of the system to catalytic conditions, thus generating the competent peroxo-POMs in situ by addition of excess  $\text{H}_2\text{O}_2$ .<sup>[26]</sup> Exploratory experiments have thus been

performed on recharging the spent reaction mixtures with a supplementary and stoichiometric amount of both  $\text{H}_2\text{O}_2$  and substrate (entries 7, 9, and 11 in Table 1). The oxidation activity was immediately restored, with analogous conversion, selectivity, and kinetics behavior for all the three systems under investigation. Superimposable time-evolution profiles for **SO** conversion and parallel **SO**<sub>2</sub> formation can indeed be observed (Figure 5 and Table 1 entries 7, 9, and 11). This finding points to the selective addition of  $\text{H}_2\text{O}_2$  to the Zr/Hf centers within the POM framework.

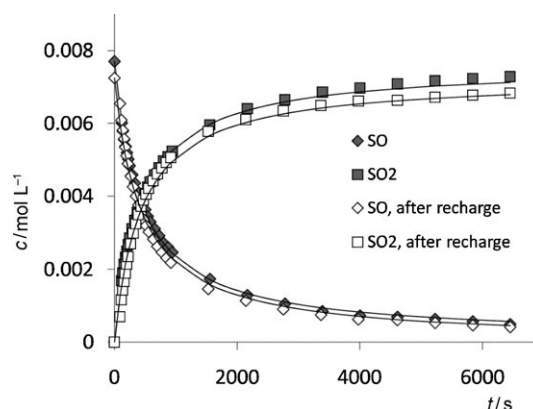


Figure 5. Oxidation of DL-methionine sulfoxide (**SO**) by **1** and recharged experiment with additional  $\text{H}_2\text{O}_2$  and substrate. In the first run, **SO** = 7.27 mM, **1** = 3.63 mM; in the recharge,  $\text{H}_2\text{O}_2$  = 7.27 mM (entries 6 and 7 in Table 1), in  $\text{D}_2\text{O}$  (500  $\mu\text{L}$ ).

Catalytic oxidation of **S** and **SO** has thus been successfully achieved in the presence of an excess of  $\text{H}_2\text{O}_2$ , yielding up to 45 turnovers, 70–99% yield, and a reactivity order **3** > **1** > **2**, in line with the stoichiometric behavior (Table 2 and Figures S37–S42 in the Supporting Information).<sup>[27,28]</sup> Vice-versa, spectroscopic analysis of spent **4** and **5** indicates a substantial modification of the POM features, and  $\text{H}_2\text{O}_2$  recharge under catalytic conditions cannot be attributed to a well-identified reactive system (Figures S35–S36 in the Supporting Information).<sup>[29]</sup>

The reaction scope in aqueous solution has been extended to alcohol oxidation catalyzed by POMs **1–3**, through a mi-

Table 2. Catalytic oxidation of L-methionine (**S**) or DL-methionine oxide (**SO**) by peroxo-POMs **1–3** and  $\text{H}_2\text{O}_2$  in aqueous solution.<sup>[a]</sup>

Sub	POM <sup>[b]</sup>	Conv [%] <sup>[c]</sup>	Time [h]	Initial rate, $R_0$ [ $\text{molL}^{-1}\text{s}^{-1}$ ] <sup>[d]</sup>
1	<b>S</b> <b>1</b> ( $\text{Zr}_2\text{Si}$ )	> 99 <sup>[e]</sup>	0.25	$2.9 \times 10^{-5}$
2	<b>S</b> <b>2</b> ( $\text{Zr}_2\text{Ge}$ )	> 99 <sup>[e]</sup>	0.5	$1.0 \times 10^{-5}$
3	<b>S</b> <b>3</b> ( $\text{Hf}_2\text{Si}$ )	> 99 <sup>[e]</sup>	0.08	$5.5 \times 10^{-5}$
4	<b>SO</b> <b>1</b> ( $\text{Zr}_2\text{Si}$ )	70 <sup>[f]</sup>	48	$5.8 \times 10^{-8}$
5	<b>SO</b> <b>2</b> ( $\text{Zr}_2\text{Ge}$ )	80 <sup>[f]</sup>	48	$6.9 \times 10^{-8}$
6	<b>SO</b> <b>3</b> ( $\text{Hf}_2\text{Si}$ )	93 <sup>[f]</sup>	20	$1.1 \times 10^{-7}$

[a] In all reactions [Sub] = 7.27 mM, [POM] = 0.16 mM, [ $\text{H}_2\text{O}_2$ ] = 7.27 mM, in  $\text{D}_2\text{O}$  (500  $\mu\text{L}$ ), at 28 °C. [b] See Figure 1 for POM abbreviations. [c] % Substrate conversion. [d] Initial oxidation rate determined for < 15% conversion by <sup>1</sup>H NMR spectroscopy. [e] Selective **SO** formation as determined by <sup>1</sup>H NMR spectroscopy. [f] Selective **SO**<sub>2</sub> formation as determined by <sup>1</sup>H NMR spectroscopy.

crowave (MW)-assisted protocol.<sup>[30]</sup> The best performance, in terms of efficiency and catalyst stability has been achieved with **2**, for the transformation of representative cyclic and benzylic secondary alcohols (Table 3).<sup>[31]</sup> Employing a

Table 3. Catalytic oxidation of alcohols by **2** and H<sub>2</sub>O<sub>2</sub> in aqueous solution.<sup>[a]</sup>

	Substrate	Product	Conv [%] <sup>[b]</sup>
1	cyclopentanol	cyclopentanone	99
2	cyclohexanol	cyclohexanone	99
3	cycloheptanol	cycloheptanone	99
4	indanol	indanone	99
5	phenylethanol	phenyl methyl ketone	80

[a] Alcohol 0.8–1.0 mmol, POM 1.6 μmol, H<sub>2</sub>O<sub>2</sub> 0.08–0.1 mmol in H<sub>2</sub>O (500 μL). Irradiation power 70 W, time 50 min, *T*<sub>bulk</sub> 90 °C, with applied compressed air. [b] % Conversion calculated by GLC analysis, on the limiting reagent H<sub>2</sub>O<sub>2</sub>.

monomodal MW lab-station, with 70 W power irradiation, selective and complete conversion of H<sub>2</sub>O<sub>2</sub> is obtained in approximately 50 min.<sup>[32]</sup> Target substrates include the aromatic indanol, which is quantitatively oxidized to the carbonyl product, a well-known intermediate for pharmaceutical and agrochemical applications. The present protocol represents a further advancement with respect to on-water catalysis and environmentally sustainable oxidations.<sup>[33,34]</sup>

Moreover, by virtue of the POM robustness and fast kinetics, the catalytic set-up can be readily implemented in a flow-mode within microfluidic devices in which the H<sub>2</sub>O<sub>2</sub> feeding can be properly tuned to match the addition/consumption rates and optimize the steady-state concentration of the competent peroxidic intermediate.<sup>[30b]</sup>

The impact of the geometry/structure of the peroxide bridge on the oxygen-transfer catalysis has been further addressed by DFT computations, including relativistic and solvent effects. The POM structures were optimized using the ZORA-BP86 functional, with TZP basis sets; a single-point calculation using a TZ2P basis set was then performed on the final geometry.<sup>[35]</sup> Due to the large size of the molecules and to the large number of heavy metals, the internal or core electrons were kept frozen (see Experimental Section). The calculated geometries are in very good agreement with the experimental ones obtained by XRD analysis,<sup>[15,16]</sup> confirming the adherence of the calculation method to the experimental data for the title compounds. A detailed comparison of relevant experimental and calculated geometric parameters is provided in the Supporting Information (Table S1).

As a first tool to investigate the electronic character of the competent peroxo moieties, the calculated map of the electrostatic potential (MEP) provides a qualitative description of the electron distribution over the polyanion. This is a direct hint on the relative nucleophilicity/basicity of the oxygen sites, which can undergo protonation in aqueous media under the catalytic regime.<sup>[25,35]</sup> As an example, the MEP of **2** is represented in Figure 6a.

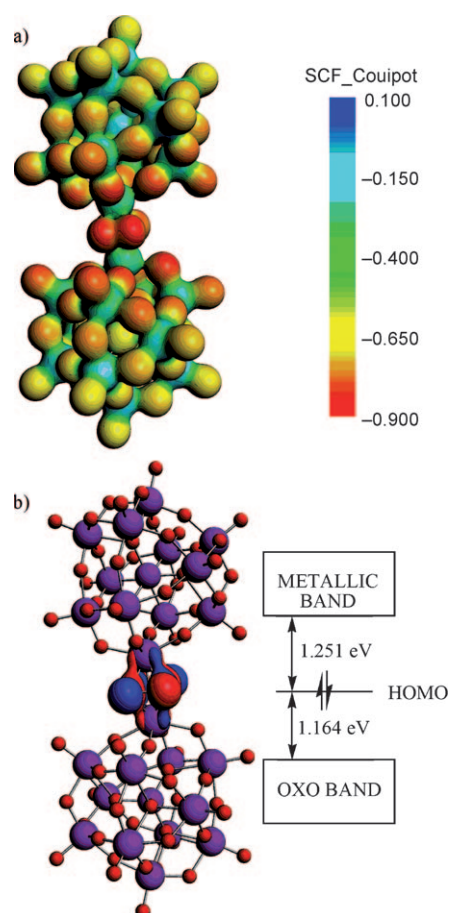


Figure 6. a) Calculated electrostatic potential surface of **2**. b) Graphical representation of the HOMO for **2**.

In general, the calculated MEP for the isostructural **1–3** clearly shows that a high electron density is localized on the peroxidic moieties and on W-O-M bridging oxygen atoms, while terminal W-O sites are relatively electron-poor.<sup>[35,36]</sup>

The molecular orbitals distribution of fully-d<sup>0</sup> POMs is generally described by two identifiable sets of molecular orbitals: the doubly occupied ones, delocalized on oxygen atoms (oxo band), and a set of virtual ones corresponding to the d orbitals of the transition metals (metallic band). In this scenario, the POM-embedded peroxo moiety gives rise to one occupied orbital, which is found half way in energy between the oxo and the metallic bands.<sup>[37]</sup> A graphical representation of the peroxo-HOMO is given in Figure 6b for **2**; a similar orbital shape is also observed for the isostructural complexes **1** and **3**. The high energy of such peroxo-HOMO orbitals and the resulting HOMO–LUMO low-energy gap stand in contrast with the strong electrophilic behavior displayed by the peroxo-POMs **1–3**, with regard to the sulfide and sulfoxide oxidation. On the other hand, the proton affinity of the peroxide moiety can be controlled by its HOMO energy. Moreover, protonation equilibria are known to trigger the electrophilic reactivity of organic and inorganic peroxides as oxygen-transfer agents.<sup>[25]</sup>

It is therefore of interest to extend this type of analysis to the trimeric peroxy-POMs **4** and **5**, which are remarkably less reactive than **1–3** (see previous discussion). While no significant changes are observed for the energies of the oxo and metallic bands, a strong difference is noticed for the peroxy-HOMOs (Figure 7), which are found at a lower

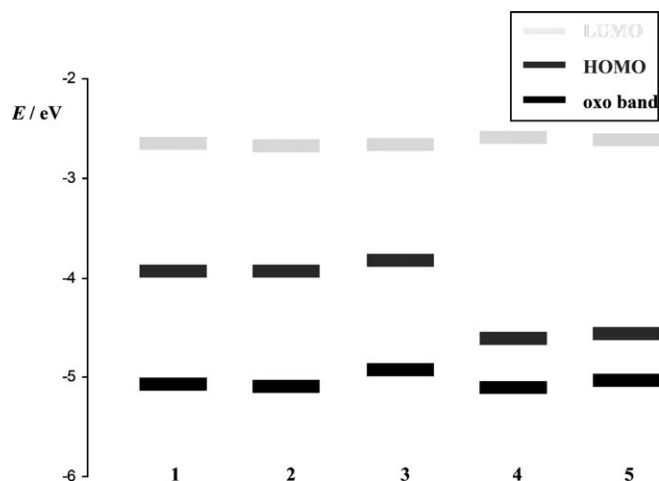


Figure 7. Frontier orbital energies calculated for **1–5**.  $E_{\text{HOMO}} = -3.934$ ,  $-3.933$ ,  $-3.827$ ,  $-4.607$  and  $-4.563$  eV for **1–5**, respectively.

energy in **4** and **5** with respect to **1–3**, by  $0.629$ – $0.782$  eV.<sup>[38]</sup> Such a result points to an enhanced proton affinity of peroxides **1–3** with respect to **4** and **5**, likely ascribed to the diverse arrangement of the  $\text{MO}_2$  moieties in the two families of complexes. Based on such evidence, the overall description of the oxygen-transfer mechanism should include possible protonation equilibria in water, which are favorable for **1–3**.

## Conclusion

Water-soluble Zr/Hf butterfly peroxy-polyoxotungstates are reactive oxidants under stoichiometric and catalytic conditions. The active core of these molecular catalysts is a mono- or bis- $\mu$ - $\eta^2$ : $\eta^2$ -peroxy ligand for each Zr/Hf center embedded within the POM scaffold. The isostructural dimers **1–3** feature two  $[\alpha\text{-XW}_{11}\text{O}_{39}]^{8-}$  ions (X=Si, Ge) linked by a  $\{\text{M}_2(\text{O}_2)_2\}^{4+}$  (M=Zr<sup>4+</sup>, Hf<sup>4+</sup>) fragment, while the derivatives **4** and **5** display a cyclic  $[\text{M}_6(\text{O}_2)_6]^{12+}$  hexameric core stabilized by three decatungstosilicate units  $[\gamma\text{-SiW}_{10}\text{O}_{36}]^{8-}$ . Analysis of oxygen-transfer to L-methionine and its sulfoxide rank the POM performance in the range  $3 \approx 1 > 2 \gg 4 \approx 5$ . In this chemistry, polyanions **1–3** behave as strong electrophiles with a reactivity ratio  $\text{S}/\text{SO} > 100$ , thus showing a major impact of the POM structure on the reactivity of the peroxide moiety. Recharging experiments proved that these POMs can be reactivated after the depletion of the peroxidic content and used for multi-turnover processes.

As frontier molecular orbital analysis addresses the difference in reactivity between polyanions **1–3** and the related complexes **4** and **5** in terms of protonation affinity of the peroxide moiety, further attention will be devoted to the effect of acidic additives in terms of catalysis rates and selectivity. To date, very few reports exist on the functional properties of Zr- or Hf-based peroxy complexes. In this regard, the unique reactivity exhibited by the totally inorganic POM-based molecular species sheds further light on the nature of transient oxidants generated on the surface of extended metal oxides applied as heterogeneous catalysts.<sup>[39]</sup>

## Experimental Section

**General procedures:** Compounds **1–5** were prepared as described elsewhere.<sup>[15,16]</sup> Commercially available L-methionine (98%), DL-methionine oxide (99%),  $\text{H}_2\text{O}_2$  (35%), and all other reagents were used as purchased without further purification. Infrared spectra were recorded on a Nicolet Avatar spectrophotometer. <sup>1</sup>H NMR spectra were recorded on a Bruker AV 300 instrument, equipped with a multinuclear probe. UV/Vis spectra were recorded with a Varian UV-NIR Cary 5000 instrument, using quartz cells with 1 cm path length. Resonance Raman spectra were acquired with a Renishaw instrument, model Invia reflex, by using the laser at 532 nm.

**Electrochemistry:** All cyclic voltammetry measurements and rotating disk experiments were performed in three-electrode systems under argon, using a potentiostat PGSTAT 20 from Autolab interfaced with a personal computer running under GPES for Windows, version 4.9 (ECO Chemie). In addition to the glassy carbon working electrode, an Ag/AgCl reference electrode (Metrohm, 6.0724.140), separated by a salt bridge containing the electrolyte was used. The scan rate was  $100 \text{ mVs}^{-1}$ . All voltammograms were recorded after 5 s of equilibration at the starting potential. The rotating disk experiments were performed with an electrode rotation speed of 3000 rpm.

**Oxidation of L-methionine and DL-methionine oxide:** In all reactions, a stock aqueous solution ( $\text{D}_2\text{O}$ ) of the substrate (37.3 mM) was diluted to match the stoichiometric content of the active peroxide (7.27 mM) in 500  $\mu\text{L}$  total volume. After total dissolution of the catalyst, (3.64 mM for **1–3** or 1.61 mM for **4** and **5**), the oxidation of **S** and **SO** was monitored by <sup>1</sup>H NMR spectroscopy ( $T=301 \text{ K}$ ), taking into account the time required to prepare the sample before spectra acquisition. Recharged experiments were performed after the reaction, by adding a new aliquot of the substrate and a stoichiometric amount of  $\text{H}_2\text{O}_2$ , to restore the initial concentrations.

**Catalytic oxidation of L-methionine and DL-methionine oxide:** A stock solution of substrate **S** or **SO** in  $\text{D}_2\text{O}$  (0.189 M) was prepared. A 3.64  $\mu\text{mol}$  sample was transferred to a 5 mm NMR tube and diluted with  $\text{D}_2\text{O}$  (500  $\mu\text{L}$ ) to obtain a final concentration of 7.27 mM. POMs **1–3** were added in the tube, using a stock solution 0.86 mM, to provide 0.081  $\mu\text{mol}$ . After the total dissolution of the catalyst, a stoichiometric amount of  $\text{H}_2\text{O}_2$  was added (7.27 mM), and the oxidation of the substrate was monitored by <sup>1</sup>H NMR spectroscopy ( $T=301 \text{ K}$ ).

**Oxidation of methionine monitored by rotating disk voltammetry:** A solution of the POMs (**1–3**,  $c_0=0.30$ – $0.64 \text{ mM}$ ) in 0.5 M HAc/KAc buffer (pH 4.7) was prepared and transferred into an electrochemical cell. L-Methionine was added in portions of 1  $\mu\text{mol}$  (**1**, **2**) or 0.5  $\mu\text{mol}$  (**3**), thus providing 7.1–14 mM (11.8–28 equiv). After total dissolution of the substrate, the reduction of the POM was monitored by CV. Initial rates, expected for the conditions employed during NMR experiments, were calculated by using bimolecular rate constants.

**Oxidation of methionine oxide monitored by CV:** A solution of the POMs (**1–3**,  $c_0=5.0 \times 10^{-4}$ – $6.0 \times 10^{-4} \text{ M}$ ) in 0.5 M HAc/KAc buffer (pH 4.7) was prepared and transferred into an electrochemical cell. DL-Methionine oxide was added, thus providing 7.1–14 mM (11.8–28 equiv). After total

dissolution of the substrate, the reduction of the POM was monitored by CV. Initial rates, expected for the conditions employed during NMR experiments, were calculated by using bimolecular rate constants.

**Catalytic oxidation of alcohols:** A 500  $\mu\text{L}$  sample of an aqueous solution containing the alcohol (0.8–1.0 mmol),  $\text{H}_2\text{O}_2$  (0.08–0.1 mmol), and catalyst (1.6  $\mu\text{mol}$ ) was poured into a MW test tube. The reaction was carried out in a monomodal MW oven, upon irradiation at 70 W and application of compressed air to avoid overheating of the sample. The reaction mixture, after checking for the presence of  $\text{H}_2\text{O}_2$  with iodinated paper, was extracted with ethyl acetate ( $4 \times 1.2 \text{ mL}$ ) and analyzed by GLC with the internal standard method.

**Computational details:** Computational resources and assistance were provided by the Laboratorio Interdipartimentale di Chimica Computazionale (LICC) at the Department of Chemical Sciences of the University of Padova. DFT calculations were carried out using the Amsterdam density functional (ADF) code;<sup>[40]</sup> scalar relativistic effects were taken into account by means of the two-component zero-order regular approximation (ZORA) method,<sup>[41]</sup> adopting the Becke 88 exchange plus the Perdew 86 correlation (BP) functional.<sup>[42]</sup> The basis functions for describing the valence electrons are triple-zeta quality, singly or doubly polarized (TZP and TZ2P, respectively), specially optimized for ZORA calculations. Due to the large size of the molecules under investigation, the internal or core electrons (O: 1s; Si: 1s to 2sp; Ge: 1s to 3spd; Zr: 1s to 4sp; Hf and W: 1s to 4spdf) were kept frozen. Geometries were optimized by taking advantage of molecular symmetry with TZP basis set; single-point calculations were then performed with TZ2P basis set. The solvent effect was modeled by means of the ADF implementation<sup>[43]</sup> of the COSMO method.<sup>[44]</sup> This method required a prior definition of atomic radii, which were set at their following recommended values (in Å): H: 1.3500; O: 1.5167; Si: 1.9083; Ge: 2.033; Zr: 2.1167; Hf: 2.1083; W: 1.9917. In addition to the dielectric permittivity  $\epsilon$ , the solvent was also modeled by an empirical parametrization of non-electrostatic solvation terms derived from the solvation of alkanes.<sup>[45]</sup> Since these parameters are currently available only for water, energies and gradients can be reliably calculated only for this solvent.<sup>[46]</sup> Therefore, all calculations assumed water as solvent.

## Acknowledgements

Financial support from CNR, MIUR, University of Padova (PRAT CPDA084893/08) and the ESF COST D40 action are gratefully acknowledged. We thank Dr. F. M. Toma for recording the resonance Raman spectra. U.K. thanks the German Research Council (Grant DFG-KO-2288/4-1), the Fonds der Chemischen Industrie, and Jacobs University for research support.

- [1] N. V. Maksimchuk, M. S. Melgunov, J. Mrowiec-Białoń, A. B. Jarzëbski, O. A. Kholdeeva, *J. Catal.* **2005**, *235*, 175–183.
- [2] a) R. Schmidt, G. Pausewang, *Z. Anorg. Allg. Chem.* **1986**, *535*, 135–142; b) C. Palazzi, L. Oliva, M. Signoretto, G. Strukul, *J. Catal.* **2000**, *194*, 286–293; c) B. N. Chernyshev, N. A. Didenko, N. G. Bakeeva, B. V. Bukvetskii, A. V. Gerasimenko, *Zh. Neorg. Khim.* **1991**, *36*, 1112–1117.
- [3] A. C. Dengel, W. P. Griffith, *Polyhedron* **1989**, *8*, 1371–1377.
- [4] a) M. T. H. Tarafder, A. R. Khan, *Polyhedron* **1991**, *10*, 819–822; b) M. T. H. Tarafder, A. R. Khan, *Polyhedron* **1991**, *10*, 973–976.
- [5] M. T. H. Tarafder, M. A. L. Miah, *Inorg. Chem.* **1986**, *25*, 2265–2268.
- [6] C. Stanciu, M. E. Jones, P. E. Fanwick, M. M. Abu-Omar, *J. Am. Chem. Soc.* **2007**, *129*, 12400–12401.
- [7] A. Falber, L. Todaro, I. Goldberg, M. V. Favilla, C. M. Drain, *Inorg. Chem.* **2008**, *47*, 454–467.
- [8] a) R. G. Finke, B. Rapko, T. J. R. Weakley, *Inorg. Chem.* **1989**, *28*, 1573–1579; b) L. Meng, J. F. Liu, *Transition Met. Chem.* **1995**, *20*, 188–190; c) A. J. Gaunt, I. May, D. Collison, K. T. Holman, M. T. Pope, *J. Mol. Struct.* **2003**, *656*, 101–106; d) X. Fang, T. Anderson, C. L. Hill, *Angew. Chem.* **2005**, *117*, 3606–3610; *Angew. Chem. Int. Ed.* **2005**, *44*, 3540–3544; e) X. Fang, T. Anderson, C. L. Hill, *Chem. Commun.* **2005**, 5044–5046; f) B. S. Bassil, M. H. Dickman, U. Kortz, *Inorg. Chem.* **2006**, *45*, 2394–2396; g) S. Yamaguchi, Y. Kikukawa, K. Tsuchida, Y. Nakagawa, K. Uehara, K. Yamaguchi, N. Mizuno, *Inorg. Chem.* **2007**, *46*, 8502–8504; h) O. A. Kholdeeva, G. M. Maksimov, R. I. Maksimovskaya, M. P. Vanina, T. A. Trubitsina, Naumov, B. A. Kolesov, N. S. Antonova, J. J. Carbó, J. M. Poblet, *Inorg. Chem.* **2006**, *45*, 7224–7234; i) R. Villanneau, H. Carabineiro, X. Carrier, R. Thouvenot, P. Herson, F. Lemos, F. R. Ribeiro, M. Che, *J. Phys. Chem. B* **2004**, *108*, 12465–12471; j) H. Carabineiro, R. Villanneau, X. Carrier, P. Herson, F. Lemos, F. Ribeiro, A. Proust, M. Che, *Inorg. Chem.* **2006**, *45*, 1915–1923; k) F. Chauveau, J. Eberle, J. Lefebvre, *Nouv. J. Chim.* **1985**, *9*, 315–320; l) A. J. Gaunt, I. May, D. Collison, K. T. Holman, M. T. Pope, *J. Mol. Struct.* **2003**, *656*, 101–106; m) Y. Kikukawa, S. Yamaguchi, K. Tsuchida, Y. Nakagawa, K. Uehara, K. Yamaguchi, N. Mizuno, *J. Am. Chem. Soc.* **2008**, *130*, 5472–5478; n) A. Falber, B. P. Burton-Pye, I. Radivojevic, L. Todaro, R. Saleh, L. C. Francesconi, C. Michael Drain, *Eur. J. Inorg. Chem.* **2009**, 2459–2466.
- [9] a) X. Zhang, C. J. O'Connor, G. B. Jameson, M. T. Pope, *Inorg. Chem.* **1996**, *35*, 30–34; b) R. Neumann, M. Dahan, *Nature* **1997**, *388*, 353–355; c) C. Nozaki, I. Kiyoto, Y. Minai, M. Misono, N. Mizuno, *Inorg. Chem.* **1999**, *38*, 5724–5729; d) U. Kortz, M. G. Save-lieff, B. S. Bassil, B. Keita L. Nadjo, *Inorg. Chem.* **2002**, *41*, 783–789.
- [10] a) M. T. Pope, *Heteropoly and Isopoly Oxometalates*, Springer, Berlin, **1983**; b) M. T. Pope in *Comprehensive Coordination Chemistry II, Vol. 4: Transition Metal Groups 3–6* (Eds.: J. A. McCleverty, T. J. Meyer), Elsevier, Oxford, **2003**, p. 635; c) C. L. Hill in *Comprehensive Coordination Chemistry II, Vol. 4: Transition Metal Groups 3–6* (Eds.: J. A. McCleverty, T. J. Meyer), Elsevier, Oxford, **2003**, p. 679.
- [11] a) O. A. Kholdeeva, B. G. Donoeva, T. A. Trubitsina, G. Al-Kadamany, U. Kortz, *Eur. J. Inorg. Chem.* **2009**, 5134–5141; b) O. A. Kholdeeva, R. I. Maksimovskaya, *J. Mol. Catal. A: Chem.* **2007**, *262*, 7–24.
- [12] a) A. Bagno, M. Bonchio, A. Sartorel, G. Scorrano, *Eur. J. Inorg. Chem.* **2000**, 17–20; b) M. Bonchio, M. Carraro, G. Scorrano U. Kortz, *Adv. Synth. Catal.* **2005**, *347*, 1909–1912; c) M. Bonchio, M. Carraro, A. Sartorel, G. Scorrano, U. Kortz, *J. Mol. Catal. A: Chem.* **2006**, *251*, 93–99; d) M. Bonchio, M. Carraro, A. Farinazzo, A. Sartorel, G. Scorrano, U. Kortz, *J. Mol. Catal. A: Chem.* **2007**, *262*, 36–40.
- [13] A. Sartorel, M. Carraro, G. Scorrano, B. S. Bassil, M. H. Dickman, B. Keita, L. Nadjo, U. Kortz, M. Bonchio, *Chem. Eur. J.* **2009**, *15*, 7854–7858.
- [14] a) A. Sartorel, M. Carraro, R. De Zorzi, S. Geremia, N. D. McDaniel, S. Bernhard, G. Scorrano, M. Bonchio, *J. Am. Chem. Soc.* **2008**, *130*, 5006–5007; b) A. Sartorel, P. Miró, E. Salvadori, S. Romain, M. Carraro, G. Scorrano, M. Di Valentin, A. Llobet, C. Bo, M. Bonchio, *J. Am. Chem. Soc.* **2009**, *131*, 16051–16053; c) M. Orlandi, R. Argazzi, A. Sartorel, M. Carraro, G. Scorrano, M. Bonchio, F. Scandola, *Chem. Commun.* **2010**, *46*, 3152–3154.
- [15] S. S. Mal, N. H. Nsouli, M. Carraro, A. Sartorel, G. Scorrano, H. Oelrich, L. Walder, M. Bonchio, U. Kortz, *Inorg. Chem.* **2010**, *49*, 7–9.
- [16] B. S. Bassil, S. S. Mal, M. H. Dickman, U. Kortz, H. Oelrich, L. Walder, *J. Am. Chem. Soc.* **2008**, *130*, 6696–6697.
- [17] F. M. Toma, A. Sartorel, M. Iurlo, M. Carraro, P. Parris, C. Maccato, S. Rapino, B. Rodriguez Gonzalez, H. Amenitsch, T. Da Ros, L. Casalis, A. Goldoni, M. Maccaccio, G. Scorrano, G. Scoles, F. Paolucci, M. Prato, M. Bonchio, *Nat. Chem.* **2010**, *2*, 826–831.
- [18] M. Carraro, A. Sartorel, G. Scorrano, C. Maccato, M. H. Dickman, U. Kortz, M. Bonchio, *Angew. Chem.* **2008**, *120*, 7385–7389; *Angew. Chem. Int. Ed.* **2008**, *47*, 7275–7279.
- [19] M. Bonchio, V. Conte, F. Di Furia, G. Modena, S. Moro, T. Carofiglio, F. Magno, P. Pastore, *Inorg. Chem.* **1993**, *32*, 5797–5799.

- [20] Experimental conditions were optimized to study only the first oxidative step of L-methionine and to guarantee the pH stability of the POM catalyst.
- [21] a) M. Bonchio, S. Calloni, F. Di Furia, G. Licini, G. Modena, S. Moro, W. A. Nugent, *J. Am. Chem. Soc.* **1997**, *119*, 6935–6936; b) M. Bonchio, V. Conte, M. A. De Conciliis, F. Di Furia, F. P. Ballistreri, G. A. Tomaselli, *J. Org. Chem.* **1995**, *60*, 4475–4480.
- [22] Blank experiment using H<sub>2</sub>O<sub>2</sub> in the absence of POM showed no significant conversion of either L-methionine or DL-methionine oxide, under the conditions explored.
- [23] a) K. Micoine, B. Hasenknopf, S. Thorimbert, E. Lacôte, M. Malacria, *Org. Lett.* **2007**, *9*, 3981–3984; b) S. Berardi, M. Carraro, M. Iglesias, A. Sartorel, G. Scorrano, M. Albrecht, M. Bonchio, *Chem. Eur. J.* **2010**, *16*, 10662–10666.
- [24] Vibrational bands for metal–peroxo bonds ( $\nu_{\text{sym}}$  and  $\nu_{\text{asym}}$  [M(O<sub>2</sub>)] stretchings, expected at about 620–650 and 545–560 cm<sup>-1</sup>, respectively) and for the O–O bond at about 820–860 cm<sup>-1</sup> (FT-IR) and 850–875 cm<sup>-1</sup> (resonance Raman) are too weak, in comparison to other POM vibrational bands, to be detected. See D. D. Agarwal, R. Jain, R. P. Bhatnagar, S. Srivastava, *Polyhedron* **1990**, *9*, 1405–1409.
- [25] a) N. S. Antonova, J. J. Carbó, U. Kortz, O. A. Kholdeeva, J. M. Poblet, *J. Am. Chem. Soc.* **2010**, *132*, 7488–7497; b) O. A. Kholdeeva, T. A. Trubitsina, R. I. Maksimovskaya, A. V. Golovin, W. A. Neiwert, B. A. Kolesov, X. López, J. M. Poblet, *Inorg. Chem.* **2004**, *43*, 2284–2292.
- [26] Catalytic oxidations of thioanisole and other substrates, with H<sub>2</sub>O<sub>2</sub> and a dendritic salt of **1** have also been successfully performed in a biphasic aqueous/CDCl<sub>3</sub> system, see: C. Jahier, S. S. Mal, U. Kortz, S. Nlate, *Eur. J. Inorg. Chem.* **2010**, 1559–1566.
- [27] A non-productive decomposition of H<sub>2</sub>O<sub>2</sub> is generally expected for Zr-based heterogeneous catalysts, see M. J. Morandin, R. Gavagnin, F. Pinna, G. Strukul, *J. Catal.* **2002**, *212*, 193–200.
- [28] The different reactivity, even in catalytic conditions, is in agreement with a selective activation of H<sub>2</sub>O<sub>2</sub> by the hetero transition metal. See W. Adam, P. L. Alsters, R. Neumann, C. R. Saha-Möller, D. Sloboda-Rozner, R. Zhang, *J. Org. Chem.* **2003**, *68*, 1721–1728.
- [29] Catalytic oxidation by **4** and **5** and H<sub>2</sub>O<sub>2</sub> proceeds with a reverse reactivity order (**4** > **5**) and poor selectivity in contrast with the stoichiometric behavior.
- [30] a) M. Carraro, L. Sandei, A. Sartorel, G. Scorrano, M. Bonchio, *Org. Lett.* **2006**, *8*, 3671–3674; b) S. Berardi, M. Bonchio, M. Carraro, V. Conte, A. Sartorel, G. Scorrano, *J. Org. Chem.* **2007**, *72*, 8954–8957.
- [31] FT-IR of the recovered catalyst confirms its stability even in such conditions (Figure S43). POMs **1** and **3** showed a decreased efficiency under identical conditions.
- [32] Under the conditions explored the blank reaction accounts for < 10% of the reactivity with a major unproductive H<sub>2</sub>O<sub>2</sub> decomposition, while the reaction with primary alcohols occurs up to 50%.
- [33] M. Carraro, A. Sartorel, G. Scorrano, T. Carofiglio, M. Bonchio, *Synthesis* **2008**, *12*, 1971–1978.
- [34] The dendrimer-like salt of POM **1**, reported in reference [26], was inactive towards the catalytic alcohol oxidation, in biphasic conditions and under milder temperature conditions.
- [35] a) A. Sartorel, M. Carraro, A. Bagno, G. Scorrano, M. Bonchio, *Angew. Chem.* **2007**, *119*, 3319–3322; *Angew. Chem. Int. Ed.* **2007**, *46*, 3255–3258; b) A. Sartorel, M. Carraro, A. Bagno, G. Scorrano, M. Bonchio, *J. Phys. Org. Chem.* **2008**, *21*, 596–602.
- [36] DFT calculations on a postulated monomeric Ti<sup>IV</sup> POM with peroxide ligand attached to Ti in a  $\eta^2$ -coordination mode, predict an analogous MEP diagram; see reference [25].
- [37] a) X. López, C. Bo, J. M. Poblet, *J. Am. Chem. Soc.* **2002**, *124*, 12574–12582; b) J. M. Poblet, X. López, C. Bo, *Chem. Soc. Rev.* **2003**, *32*, 297–308.
- [38] In **4** and **5**, six occupied orbitals with very similar energies are localized on the six peroxidic moieties (HOMO to HOMO–5); the energy mentioned in the discussion relates to the HOMO.
- [39] O. A. Kholdeeva, *Topics in Catalysis* **2006**, *40*, 229–243.
- [40] G. te Velde, F. M. Bickelhaupt, E. J. Baerends, C. Fonseca Guerra, S. J. A. van Gisbergen, J. G. Snijders, T. Ziegler, *J. Comput. Chem.* **2001**, *22*, 931–967.
- [41] a) S. K. Wolff, T. Ziegler, E. van Lenthe, E. J. Baerends, *J. Chem. Phys.* **1999**, *110*, 7689–7698; b) J. Autschbach in *Calculation of NMR and EPR Parameters: Theory and Applications* (Eds.: M. Kaupp, M. Bühl, V. G. Malkin), Wiley-VCH, Weinheim, **2004**, Chapter 14; c) E. van Lenthe, E. J. Baerends, J. G. Snijders, *J. Chem. Phys.* **1993**, *99*, 4597–4610; d) E. van Lenthe, Ph.D. Thesis, Vrije Universiteit, Amsterdam (The Netherlands), **1996**.
- [42] a) A. D. Becke, *Phys. Rev. A* **1988**, *38*, 3098–3100; b) J. P. Perdew, *Phys. Rev. B* **1986**, *33*, 8822–8824.
- [43] C. C. Pye, T. Ziegler, *Theor. Chem. Acc.* **1999**, *101*, 396–408.
- [44] a) A. Klamt, G. Schüürmann, *J. Chem. Soc. Perkin Trans. 2* **1993**, 799–805; b) A. Klamt, V. Jones, *J. Chem. Phys.* **1996**, *105*, 9972–9981; c) A. Klamt, *J. Phys. Chem.* **1995**, *99*, 2224–2235.
- [45] T. N. Truong, E. V. Stefanovich, *Chem. Phys. Lett.* **1995**, *240*, 253–260.
- [46] Thermodynamics of solvation of hydrocarbons are profoundly different according to whether the solvent is water or any other liquid. W. Blokzijl, J. B. F. N. Engberts, *Angew. Chem.* **1993**, *105*, 1610–1650; *Angew. Chem. Int. Ed. Engl.* **1993**, *32*, 1545–1579.

Received: October 27, 2010  
Published online: June 8, 2011